High-latitude ionospheric electrostatic turbulence studied by means of the wavelet transform

Dominique Lagoutte, Jean-Claude Cerisier, J.L. Plagnaud, Jean-Paul Villain, Benoît Forget

High-latitude ionospheric electrostatic turbulence studied by means of the wavelet transform

D. LAGOUTTE,* J. C. CERISIER,† J. L. PLAGNAUD,† J. P. VILLAIN* and B. FORGET†

* Laboratoire de Physique et Chimie de l'Environnement, 3A avenue de la recherche scientifique, 45071 Orléans cedex, France; † Centre de Recherches en Physique de l'Environnement, 4 avenue de Neptune, 94107 Saint Maur des Fossés cedex, France

Abstract—The wavelet transform, after performing a time-scale decomposition by means of wavelet coefficients, displays the energy of a signal simultaneously in time and frequency. According to the uncertainty principle, at each frequency an optimal compromise between time resolution and frequency resolution is provided. The Morlet (complex-valued) wavelet is applied to the study of high-latitude electrostatic turbulence recorded onboard the AUREOL-3 satellite. The transforms of electron density and of one electric field component (approximately perpendicular to the Earth's magnetic field) are presented. The modulus of wavelet coefficients show vertical structures that are due to intensifications of the signal at a high frequency occurring at the same time as at a low frequency. At each frequency, the duration of a turbulent event is of the order of a few periods, which implies that electrostatic turbulence is highly inhomogeneous. We can compare the two signals by calculating the ratio of the modulus of their wavelet transform and the phase difference. This comparison illustrates the differences between the frequency–time behaviours of the two fields, which are probably related to the nonlinear regime of turbulence.

1. INTRODUCTION

In recent years, a high-latitude ionospheric plasma turbulence has received considerable attention. Since the initial measurements by KELLEY and MOZER (1972) of correlated electric and density fluctuations poleward of the plasmapause, numerous authors have reported spacecraft and ground observations of turbulence. Among these, TEMERIN (1978) has shown that these fluctuations are polarized perpendicular to the static magnetic field and that their phase velocity is close to zero in the plasma frame. This corresponds to frozen turbulence. When observed onboard a moving spacecraft, the data are fluctuations in the time domain. The observed frequency is a Doppler-shifted frequency due to the movement of the spacecraft relative to the plasma.

Several authors have recently reviewed the theoretical aspects of fluid turbulence in the ionosphere (KINTNER and SEYLER, 1985; TSUNODA, 1988). In the wavelength range of interest in this study (between 100 m and 10 km), the gradient drift instability has been identified as the main source of plasma structure (CERISIER *et al.*, 1985). In auroral arcs, narrow zones of shear driven turbulence are observed with intense electric field fluctuations (BASU *et al.*, 1988).

In the nonlinear regime, the power spectrum of the turbulence has been shown to be close to power laws characterized by a spectral index (the slope of the spectrum in logarithmic coordinates) and in good agreement with experimental results (KESKINEN and OSSAKOW, 1983). However, electrostatic turbulence is a non-stationary phenomenon. The description of this non-stationarity is essential, inasmuch as it is directly linked to the spatial inhomogeneity of the turbulence. The usual method is to decompose the signal in a two-dimensional space, displaying the wave energy as a function of time (or space) and of frequency (or wavelength). The interest of this description is that it potentially allows one to study the connection between the different scales which exist simultaneously in the plasma. Furthermore, it can provide information on the nature of the cascading processes, which are believed to operate in the nonlinear regime.

Different representations are mostly used. The first one, called the time-windowed Fourier transform, is obtained by dividing the signal into successive time intervals of constant duration, during which the signal is assumed to be stationary. The GABOR (1946) representation, in particular, is obtained when the signal is windowed by a gaussian function. The main handicap of such a technique is that time resolution and frequency resolution are kept constant, which makes it difficult to study simultaneously phenomena which occur at different scales. The way to overcome this difficulty is to increase the time resolution with fre-

quency. This leads to the 'constant-Q short-time spectral analysis' (FLANDRIN, 1990a), which is the fundamental characteristic of any wavelet analysis developed initially by Morlet (GOUPILLAUD *et al.*, 1984). The wavelets $g_{b,a}(t)$ are built from an analysing wavelet $g(t)$ by time translation with a delay b and time dilatation by a factor $1/a$. The aim of the wavelet transform is to decompose an arbitrary signal into localized elementary contributions in both time and scale (the latter word is more general than frequency and applies to any wavelet). The dilatation parameter governs the scale analysis and allows one to study phenomena simultaneously with very different scales. The wavelets of the Morlet family, which are modulated gaussians, realize the constant-Q analysis with the optimal window shape of Gabor. Within the uncertainty principle, they also offer the possibility of adjusting the equilibrium between the time and frequency resolutions by changing the modulation frequency.

The aim of this paper is to evaluate the potential interest of the wavelet analysis for the study of ionospheric and, more generally, plasma turbulence. The paper is organized as follows. First the basic definitions about the wavelet transform are introduced and the wavelet coefficients are normalized to give time–frequency spectrograms in physical units. The notion of an optimal compromise between time and frequency resolutions is also given in a quantitative meaning. In Section 3, the wavelet transform (Morlet wavelet) is applied to the turbulent signal measured by the AUREOL-3 satellite in the high-latitude ionosphere. The signals are one component of the electric field fluctuation and the simultaneous electron density fluctuation. Finally, Section 4 is devoted to a discussion of the results and their physical meaning. It is shown, in particular, how the wavelet analysis leads to a description of the relation between the different scales and of a characterization of the inhomogeneity of the turbulence.

2. THE WAVELET TRANSFORM

In this section, we develop the basic concepts of the wavelet transform. A more detailed presentation of the wavelet transform can be found in GROSSMAN *et al.* (1990), GOUPILLAUD *et al.* (1984) and the references in both papers.

2.1. *Basic definitions*

Let $g(t)$ be a complex-valued function. To be called an analysing wavelet, it cannot be chosen arbitrarily and must fulfil a set of conditions, the more important of which are:

—$g(t)$ has a finite energy $\int |g(t)|^2 \, dt < +\infty$.
The vertical bars denote the modulus. A plane wave does not have a finite energy and thus cannot be an analysing wavelet.

—$g(t)$ has zero-mean value $\int g(t) \, dt = 0$.
This leads $g(t)$ to be an oscillating function (at least over several oscillations).

—$g(t)$ satisfies the admissibility condition $\int |G(\omega)|^2/\omega \, d\omega < +\infty$ where $G(\omega)$ is the Fourier transform of $g(t)$ defined as:

$$G(\omega) = \int_{-\infty}^{+\infty} g(t) \, e^{-j\omega t} \, dt. \tag{1}$$

If $G(\omega)$ is differentiable, the above condition implies that $G(\omega)$ has no d.c. component (i.e. $G(0) = 0$), which is not independent from the zero mean value.

From the analysing wavelet $g(t)$, a family of wavelets $g_{b,a}(t)$ is generated by time translation indexed by the parameter b, and by time dilatation (or contraction) indexed by the parameter a. For $a \ll 1$, the wavelet $g_{b,a}(t)$ is strongly concentrated in time and contains small scales; conversely, for $a \gg 1$, the wavelet spreads out and contains mostly large scales. The general function of that family is:

$$g_{b,a}(t) = \frac{1}{\sqrt{a}} g\left(\frac{t-b}{a}\right) \quad b \in \mathbb{R}, a > 0 \tag{2}$$

where the factor $1/\sqrt{a}$ ensures that the energy is conserved between the wavelets corresponding to different values of the dilatation factor.

The wavelet transform of a real time-dependent signal $x(t)$ is a continuous function $C(b, a)$ given by convolution of the signal with the dilated wavelet:

$$C(b,a) = \frac{1}{\sqrt{a}} \int_{-\infty}^{+\infty} x(t) g^*\left(\frac{t-b}{a}\right) dt \tag{3}$$

where $g^*(t)$ is the complex conjugate of $g(t)$.

Another way to calculate the wavelet transform is with the help of the Fourier transforms of the signal $x(t)$ and of the analysing wavelet $g(t)$:

$$C(b,a) = \sqrt{a} \int_{-\infty}^{+\infty} G^*(a\omega) \, e^{j\omega b} X(\omega) \, d\omega. \tag{4}$$

The transform $C(b, a)$ has properties that make it a practical tool for signal analysis. The total energy of the signal can be found from the wavelet transform, since it satisfies Parseval's relation of energy conservation:

$$\int_{-\infty}^{+\infty} x^2(t)\,\mathrm{d}t = \frac{1}{K_g}\int_{-\infty}^{+\infty}\int_{-\infty}^{+\infty}\frac{1}{a^2}|C(b,a)|^2\,\mathrm{d}a\,\mathrm{d}b \qquad (5)$$

where K_g is a constant that depends only on the analysing wavelet and is given by the following relation, which justifies the admissibility condition:

$$K_g = \int_0^{+\infty}|G(\omega)|^2\frac{\mathrm{d}\omega}{\omega}. \qquad (6)$$

The signal $x(t)$ can be reconstructed from $C(b, a)$. More details about the inverse method of the wavelet transform are given by DAUBECHIES (1990).

2.2. *The Morlet wavelet*

The Morlet wavelet (GOUPILLAUD *et al.*, 1984) is a continuous and complex-valued modulated gaussian, thus giving modulus and phase in the spectral domain. We have selected this type of wavelet for two main reasons. First, a gaussian function gives the smallest time–bandwidth product (PAPOULIS, 1977). Second, a simple relation exists between scale and frequency relations that will be further explained in Section 2.3. The Morlet wavelet is expressed by:

$$g(t) = \mathrm{e}^{j\omega_0 t}\,\mathrm{e}^{-t^2/2} - \sqrt{2}\,\mathrm{e}^{-\omega_0^2/4}\,\mathrm{e}^{j\omega_0 t}\,\mathrm{e}^{-t^2}. \qquad (7)$$

The second term in $g(t)$ maintains the zero-mean value. For $\omega_0 > 5$, this term is much smaller than the first one and can be neglected. From now on, we shall use the simplified expression:

$$g(t) = \mathrm{e}^{j\omega_0 t}\,\mathrm{e}^{-t^2/2} \qquad (8)$$

with a Fourier transform:

$$G(\omega) = \sqrt{2\pi}\,\mathrm{e}^{-[(\omega-\omega_0)^2]/2}. \qquad (9)$$

This expression is maximum for $\omega = \omega_0$, which is located on the positive frequency side or on the negative frequency side, according to the sign of the wavelet pulsation ω_0. For instance, with a scale parameter $a > 0$ and a wavelet pulsation $\omega_0 > 0$, only the positive frequencies of the Fourier component $X(\omega)$ will play a significant role in equation (4) to calculate the transforms $C(b, a)$. More generally, DAUBECHIES (1990) shows that this result is valid for wavelets with an even Fourier transform. For a complex-valued signal $x(t)$, the transform $C_{\omega>0}(b, a)$ at positive frequencies is calculated with $\omega_0 > 0$, and the transform $C_{\omega<0}(b, a)$ at negative frequencies with $\omega_0 < 0$. For a real-valued signal, we can consider only the positive frequencies ($\omega_0 > 0$) that are analogous with the one-sided spectral density functions (BENDAT and PIERSOL, 1971). Introducing the relation $X^*(\omega) = X(-\omega)$, we find $C_{\omega>0}(b, a) = C^*_{\omega<0}(b, a)$. So, as with a classical Fourier transform, half of the total power is supported by the negative frequencies. Consequently, the wavelet transform will be calculated with $\omega_0 > 0$ and we adopt the formalism:

$$C(b,a) = \sqrt{2}\int x(t)g^*_{b,a}(t)\,\mathrm{d}t \quad \omega\in[0,+\infty]$$

$$C(b,a) = 0 \qquad \omega\in[-\infty,0]. \qquad (10)$$

2.3. *Scale-frequency conversion*

In spectral analysis of geophysical signals, the usual representation is in the time–frequency plan, for which it is necessary to convert scale a into frequency f. The frequency localization of the Morlet wavelet can be deduced from the maximum of the Fourier transform of its dilated form given by relation (2), which is centred around the frequency (FLANDRIN, 1990b):

$$f = \frac{f_0}{a} \qquad (11)$$

and that represents the 'instantaneous frequency' of the time-scaled wavelet (derivative of the phase with respect to time).

As, at each time b, the integrated power over scale is equal to the integrated power over frequency:

$$\frac{1}{K_g}\int_{-\infty}^{+\infty}\frac{1}{a^2}|C(b,a)|^2\,\mathrm{d}a = \frac{1}{K_g}\int_{-\infty}^{+\infty}\int_{-\infty}^{+\infty}\frac{1}{f_0}\times|C(b,f_0/f)|^2\,\mathrm{d}f$$

and more as normalized quantities have to be used to give a physical meaning to the coefficients, we defined the normalized wavelet coefficients $H(b, f_0/f)$ by:

$$H(b,f_0/f) = \frac{1}{\sqrt{K_g f_0}}\,C(b,f_0/f). \qquad (12)$$

Parseval's relation now becomes:

$$\int_{-\infty}^{+\infty}x^2(t)\,\mathrm{d}t = \int_0^{+\infty}\int_{-\infty}^{+\infty}|H(b,f_{t0}/f)|^2\,\mathrm{d}f\,\mathrm{d}b. \qquad (13)$$

The coefficients $H(b, f_0/f)$ are complex-valued. The modulus gives the distribution of the energy density in the frequency–time plane, while the isophase lines in this plane converge towards the most irregular parts (or singularities) of the signal (KRONLAND-MARTINET *et al.*, 1987).

2.4. *Discretization*

The previous definitions are made for continuous signals. In practice, however, one works with sampled signals obtained from $x(t)$ by measurements at the

instants $t_n = n\Delta t$, where $f_e = 1/\Delta t$ is the sampling frequency. We chose to discretize the frequency $f_m = f_M a_0^{-m}$, where f_M is the maximum frequency that we wanted to analyse ($f_M \leqslant f_e/2$). Thus the dilatation parameter is $a_m = f_0/f_M a_0^m$. Increasing values of the frequency index m represent more spread-out wavelets. We discretized the translation step so that it is proportional to the width of the wavelet at each frequency, by choosing $b_k = k a_m b_0$. The parameters a_0 and b_0 ($a_0 > 1$, $b_0 \geqslant 0$), which define the sampling of the wavelet transform, will be explained at the end of this section. Therefore, formula (12) should be replaced by its discrete version taking into account the normalization:

$$H(k,m) = \frac{\Delta t\sqrt{2}}{K_g f_0} \sum_n x(n\Delta t) a_0^{-m/2} \left(\frac{f_M}{f_0}\right)^{1/2} \times g(n\Delta t a_0^{-m} - k b_0). \quad (14)$$

The discretization step in frequency (δf) is given by:

$$\frac{\delta f}{f} = 1 - a_0^{-1} = cte$$

which shows that δf is proportional to the frequency. The discretization step in time δb is linked to δf by:

$$\delta b \cdot \delta f = b_0 f_0 (1 - a_0^{-1}) = cte.$$

We now have to select the elementary steps in scale a_0 and time b_0 in such a way that they cover the entire time–frequency plane. The choice is guided by practical considerations of continuity of the time–frequency representation. A lattice containing N_f points per octave and $1/\gamma$ points per fundamental wavelet period $T_0 (T_0 = 1/f_0)$, defines the parameters a_0 and b_0:

$$a_0 = 2^{1/N_f}, \quad b_0 = \gamma T_0. \quad (15)$$

When the spectrum of the signal covers a large number of octaves (for example in audioacoustics with more than 10 octaves), the implementation of formula (14) turns out to be suitable for normal computer work. In this case, an appropriate algorithm is necessary (HOLSCHNEIDER *et al.*, 1989).

The wavelet decomposition can be made on an orthonormal basis. The terminology 'orthonormal basis' means that the signal decomposition into wavelets is unique and that the wavelet coefficients are independent. In other words, the wavelet coefficients $H(k, m)$ are not correlated. In the continuous case, knowing a signal is equivalent to knowing the function $C(b, a)$, but this is no longer automatically true for a discrete signal and its discrete set of coefficients $H(k, m)$. Several conditions on the basic wavelet $g(t)$, and parameters a_0 and b_0 are required. These conditions lead to construct wavelets which do not permit a good localization in the time–frequency plane and, consequently, these wavelets are not useful for signal analysis (DAUBECHIES, 1990). For practical purposes, it is preferable to work with functions $g(t)$ that are concentrated in time and/or in frequency, such as the Morlet wavelet. DAUBECHIES (1990) provided an algorithm that can be applied to any wavelets, to reconstruct with acceptable accuracy the initial signal from the wavelet coefficients, the accuracy being dependent on the values of the increments a_0 and b_0.

2.5. *Time and frequency resolutions of the Morlet wavelet*

From (9) and from the dilatation formula (2), we can calculate the frequency resolution at 3 dB (corresponding to an amplitude ratio $= \sqrt{2}$):

$$\frac{\Delta f}{f} = \frac{1.67}{\omega_0}.$$

This relation shows that, contrary to the Fourier transform, the frequency resolution of the wavelet transform is proportional to the frequency itself. The relative frequency resolution can be adapted to the physical problem by the correct choice of the value of the wavelet pulsation ω_0. For the 'classical Morlet wavelet' ($\omega_0 = 5.34$ which means that the amplitude decreases to half its maximum value in one period of the wavelet), the relative frequency resolution is:

$$\frac{\Delta f}{f} = 0.31.$$

If one also defines the duration ΔT of the wavelet by its -3 dB amplitude relative to its center, one obtains:

$$\Delta T = \frac{1.67\,\omega_0}{2\pi f}.$$

For the 'classical Morlet wavelet', ΔT is equal to $1.42/f$.

3. APPLICATION TO TURBULENT ELECTRIC FIELD AND ELECTRON DENSITY FLUCTUATIONS

We have chosen to apply the wavelet transform to the study of the fluctuations of the electron density and the ELF electric field, which characterize the turbulent structure of the ionospheric plasma. The experimental data were recorded onboard the AUREOL-3 satellite. The satellite, placed into a quasi-polar orbit (apogee: 2000 km, perigee: 400 km, inclination:

82.5°, period: 109.5 min), was three-axis stabilized with its z axis close to the vertical.

The electron density was obtained from the ISOPROBE experiment (BÉGHIN *et al.*, 1982), which was based on the mutual impedance probing technique. Density fluctuations along the orbit can be deduced with a time resolution of 1 ms in the fastest mode.

The ELF–VLF wave characteristics are given by the multicomponent TBF-ONCH experiment (BERTHELIER *et al.*, 1982). Three magnetic and two electric waveforms of the a.c. field were measured in the frequency range 10–1500 Hz. The electric component used in this paper (called E_H) is almost horizontal and perpendicular to the satellite velocity. At high latitude, this component is also approximately perpendicular to the Earth's magnetic field.

The data discussed in this paper were recorded on 10 March 1982 (orbit 2242) at 1740:29.500 UT. The geophysical parameters of this particular event were: invariant latitude 73.2°, geographic latitude 79°, geographic longitude 70.2°, altitude 410 km, 2330 local time. As is usual with satellite data, a time variation measured in the satellite frame can also be considered as a space variation, Doppler-shifted by the orbital motion of the satellite. The frequency f is then related to the wavelength λ of the structure by $f = V_s/\lambda$, where V_s is the satellite velocity (about 8 km·s^{-1}).

For this study, the wavelet pulsation is $\omega_0 = 5.34$, which appears to be the best compromise in order to achieve a good time resolution together with a sufficient frequency resolution. The frequency range covers six octaves with a maximum frequency of 320 Hz, which is close to the upper frequency limit of electrostatic turbulence observed onboard AUREOL-3 satellite. The number of frequencies per octave is $N_f = 8$ and the parameter γ is equal to 0.25. The wavelet transform is applied to a 1 s period of electron density N_e and electric field data E_H (Fig. 1).

The coefficients are normalized so that standard units are obtained. For example, we analyse a component of the electric field, the unit of which is volts per meter ($\equiv$ V m^{-1}). The dilatation parameter is without unit, the time parameter is in seconds ($\equiv$ s). The normalized wavelet coefficients calculated for the electric field from equation (14) are expressed in V m^{-1} Hz$^{-1/2}$. Similarly, the relative density coefficients are expressed in Hz$^{-1/2}$.

In Fig. 1, the time–frequency diagrams show the square modulus of the wavelet coefficients and the top panels show the waveform of the signals. Both signals are highly non-stationary. The mean value of the electron density is around 4.3 10^5 cm^{-3}. It shows abrupt variations of less than 5%. The mean value of the electric field component is around 0.15 mV/m. Although the waveforms look very different, the time–frequency distributions are similar, with maxima at the same time and frequency. As the frequency increases the power generally decreases, with a maximum value around 10 Hz. Vertical structures appear in the diagram which are narrowing and forking, principally following the edges of the large scale structures. For each diagram, electric field and density, the frequency width of the structures is much larger than the frequency resolution of the analysing wavelet ($\Delta f/f \approx 30\%$ for the classical Morlet wavelet as it was shown in Section 2.5). In other words, intensifications of the signal at high frequency occur at the same time as those at low frequency. Concerning the width in time of the structures in the time–frequency diagrams of Fig. 1, the duration of a turbulent event is at most a few periods, which corresponds to the time resolution of the wavelet analysis. If we translate this result into the space domain, we observe that the spatial extension of turbulence is only a few wavelengths. Especially at higher frequencies (or smaller scale structures), the turbulence appears as very localized and isolated structures.

The characteristics of these diagrams can be appreciated if we refer to the equivalent diagram, which should be produced by the analysis of a stationary white noise (see for instance GROSSMANN *et al.*, 1987). In the latter case, the dimensions of the structures are equal to the resolution of the analysis, both in time and in frequency. Furthermore the patches are uniformly spread over the diagram. Note that the phase of the wavelet transform is not easy to interpret.

Two experimental signals that belong to the same physical phenomenon can be compared through the relations between their wavelet coefficients. In Fig. 2, the ratio of the amplitudes of the coefficients (on the left) and their phase difference (on the right) are shown. The power ratio is mainly of the order of 10 mV^2 m^{-2} (yellow in the colour plot on the left of Fig. 2). Strong fluctuations around that value are observed, which can reach a factor of 10 in a specific area of the time–frequency plane. At low frequencies (less than $\approx$15 Hz, which corresponds roughly to the maximum power of electron density), the ratio is relatively uniform except for several holes corresponding to low values of E_H power. Above $\approx$15 Hz, the power ratio presents elongated structures of a few periods wide, which resemble those of the power distribution.

One has to be careful in the interpretation of the phase difference diagram because of discontinuities in the phase of the wavelet coefficients occurring at zeros of the modulus. These points are indicated in white in

the two diagrams of Fig. 2. We can observe that the phase difference is constant over several periods, confirming that both E_H and N_e belong to the same physical process. For some vertical structures, the same phase difference is observed along the structures over several octaves.

If the wavelet transform can provide more information about turbulence than a classical Fourier method, it can also give the same results as can be deduced from power spectrum analysis. Spectral indices (slope of the spectra in logarithmic coordinates) deduced from the wavelet analysis, have been compared with those computed from a classical Fourier transform for the same data sample of Fig. 1. In the wavelet analysis, the square modulus of the wavelet coefficients are time averaged at each frequency over the 1 s period. In the Fourier analysis, the transform is performed over the 1 s period. In order to calculate by a least-square method the slope of the logarithmic power spectrum, we have to average the Fourier coefficients proportionally to the frequency itself. In this case a moving average is made over a number of frequencies $m = 7 \times (\mathrm{INT}\{f/25\} + 1)$, where INT denotes the integer part. This solution gives a frequency resolution of the same order as for the wavelet transform. The results are presented for both density and electric fluctuations in Fig. 3. The calculated power spectra compare extremely well. The powers are almost identical and most of the features observed through the FFT are also present in the wavelet spectrum.

Spectral slopes computed between 12 and 180 Hz are close. The slightly shallower slope of the wavelet spectra of density fluctuations is due to somewhat larger power at high frequencies. For this turbulent event, the power spectral indices of the electron density and electric field fluctuations are almost identical, taking into account the error bounds.

4. DISCUSSION

The turbulence event presented in Figs 1–3 has been observed in the polar cap at an invariant latitude of 73° in the night time sector (2330 MLT). For this specific event, the instability responsible for the turbulence has been identified as the gradient-drift instability (Mounir *et al.*, 1991), which destabilizes a convection density gradient when the angle between the gradient and the convection velocity is smaller than 90°. Tsunoda (1988) has shown that the gradient-drift instability is the dominant instability mechanism in the high-latitude ionosphere and in the short wavelength regime ($\lambda < 10$ km). We will now discuss what new information the wavelet analysis brings to the study of the fine structure of the turbulence.

The wavelet analysis allows us to obtain the same results as the Fourier method, in particular for the power spectra. We have shown that, at least for power law spectra that are the usual method of analysing turbulent fields, both methods of analysis give the same value of the spectral index. We have confirmed for this particular event that the spectral indices of the electric field and of the density fluctuations are equal. It was shown by Cerisier *et al.* (1985) that the equality of these two spectral indices shows that the plasma is not in the diffusive regime, which occurs when the instability source has disappeared. However, one has to be careful in the interpretation of the wavelet spectra, because of the inability of the method to describe the sharp features of a power spectrum, due to the relatively large bandwidth of the wavelet and especially for low values of the ω_0 parameter.

The vertically elongated structures present on both diagrams of Fig. 1, with a time dimension of the order of the time resolution of the analysis, but extending over a frequency range much larger than the frequency resolution of the analysis, lead to several interpretations concerning the physical properties of the turbulence.

1. The turbulence is highly inhomogeneous in the time domain or in space if we assume, as it is the case for the linear theory of the gradient-drift instability or in numerical simulations of the nonlinear state (Keskinen and Ossakow, 1983), that the turbulence is stationary in the plasma frame. The resolution of the wavelet analysis of the order of 0.15 s at 10 Hz and 0.05 s at 30 Hz, which corresponds to the duration of the increases in the modulus of the wavelet coefficients. So, the first characteristic of the turbulence is its inhomogeneity in space at all wavelengths.

2. The time periods of intensification of the turbulence in the low (5–20 Hz) range, which occur between 0.0 and 0.1 s and also between 0.5 and 0.8 s, correspond to an increase in the turbulence level in the 40–80 Hz range, although, as discussed previously, the turbulence is more structured in the high frequency range. This simultaneity in the occurrence of an increased turbulence level over the whole spectrum is coherent with the cascading process, in which the short wavelengths develop on the gradients associated to longer wavelength turbulence,

3. From Fig. 1 it can be deduced that the maxima in the electric field and in the electron density are generally co-located in the low frequency range (below 25 Hz) as well as in the elongated structures occurring at high frequencies. For example, the maxima at 10 Hz

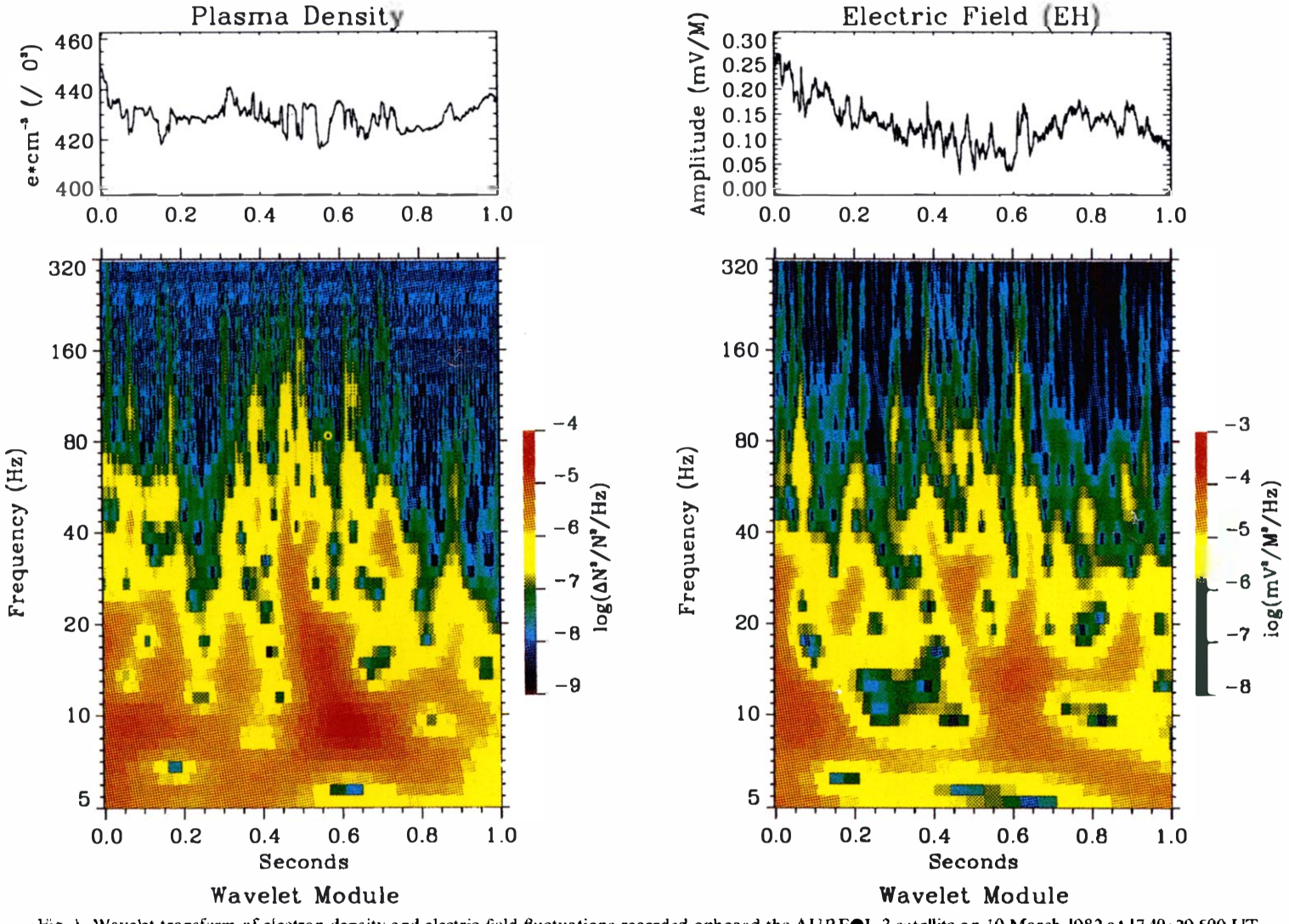

Fig. 1. Wavelet transform of electron density and electric field fluctuations recorded onboard the AUREOL-3 satellite on 10 March 1982 at 17:40:29.500 UT. The main wavelet parameters are : Morlet wavelet pulsation $\omega_0 = 5.34$ and $\gamma = 0.25$ (ratio between time increment and wavelet period). Upper panels show the waveforms. The time-frequency representations of the square modulus of wavelet transforms of electron density fluctuations (on the left) and of E_H electric field component fluctuations (on the right) are represented in colour plots. Frequency, in ordinate, is in a logarithmic scale, while time, in abscissa, is in a linear scale. A logarithmic colour scale is used for the modulus representation.

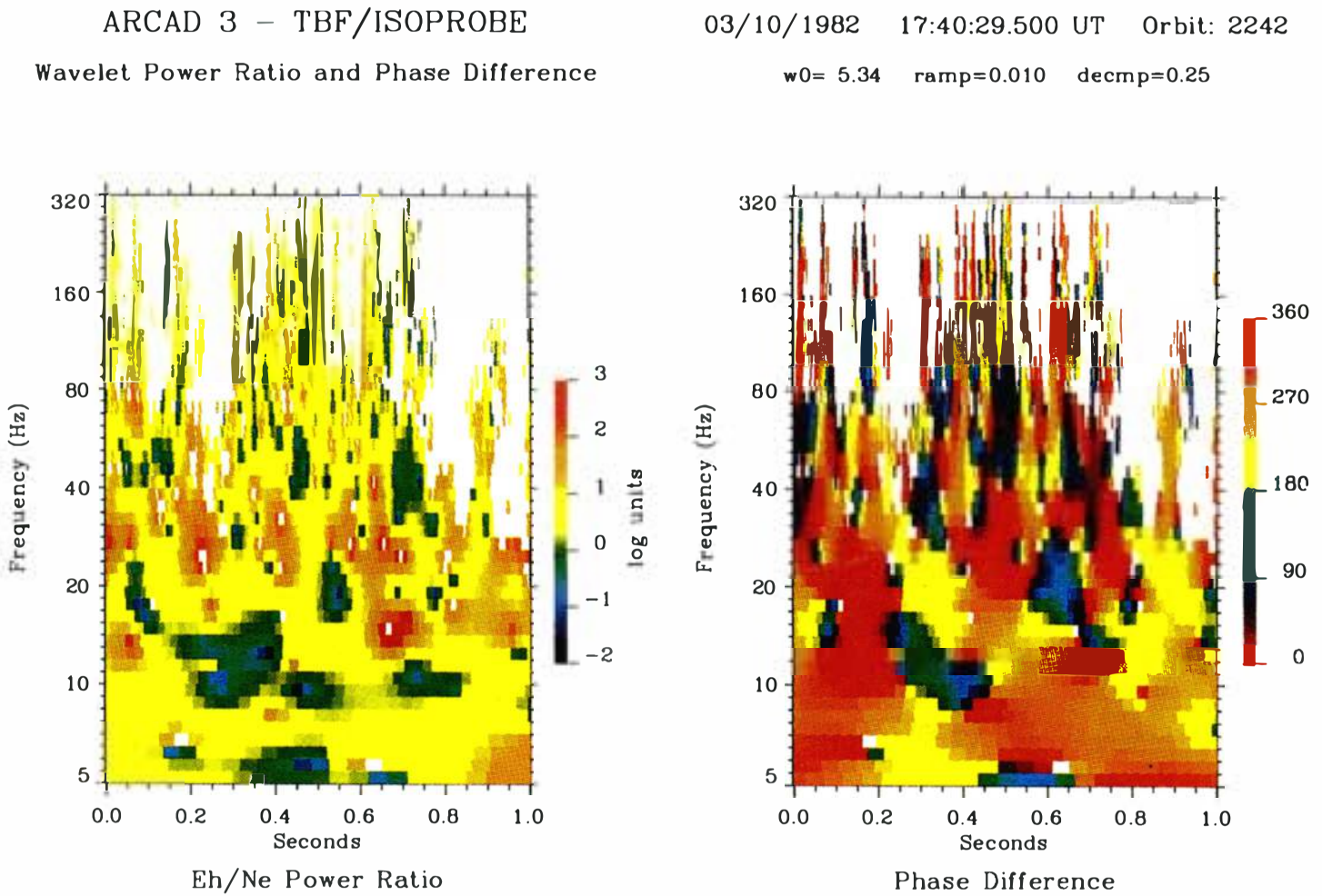

Fig. 2. Power ratio and phase difference of wavelet transforms of the E electric field component and of electron density fluctuations. A logarithmic colour scale is used for the ratio panel. Power ratio and phase difference are not shown when the respective powers of each quantity are too weak.

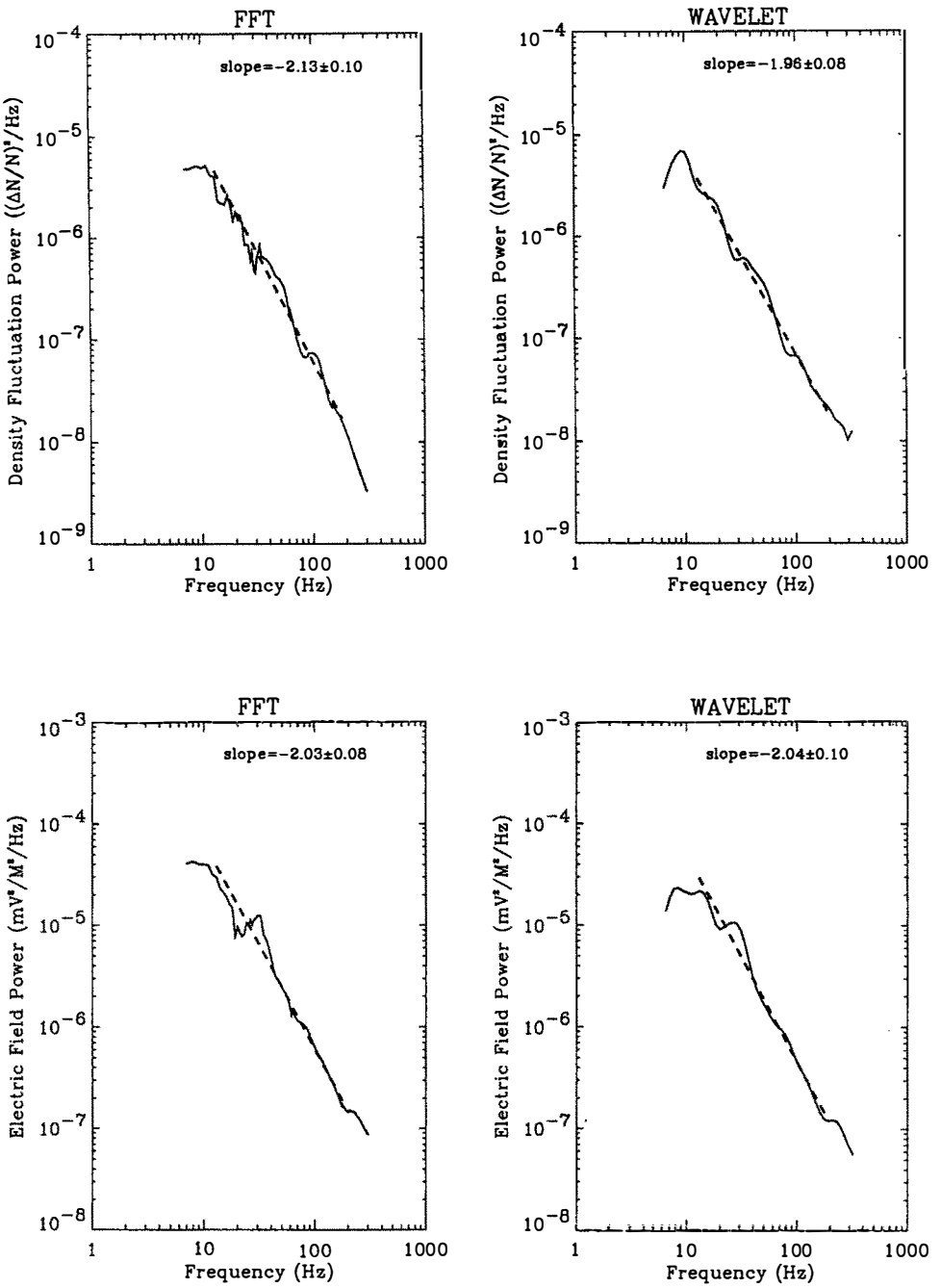

Fig. 3. Comparison between FFT power spectra and the time-averaged wavelet square modulus. The two upper panels show the power spectra of electron density fluctuations, while the two lower ones represent the power spectra of E_H electric field component. Power spectra are calculated from FFT analysis (on the left) and wavelet transform (on the right) over 1 s data presented in Fig. 1.

are simultaneously observed at 0.05 and 0.6 s for both fields, and have a phase difference (Fig. 3) taking well defined values in the range 270–300°. A third local maximum at 30 Hz and 0.47 s exhibits a phase difference close to 0°. The elongated structures generally also have a constant phase difference over more than one octave, as can be observed at 0.9 s above 30 Hz. This kind of feature could, for example, be regarded as the signature of the plasma instability mechanism (namely the gradient-drift instability) acting on the plasma in the growing phase of turbulence development. A more extended study over a larger data set is certainly needed before one can draw definitive conclusions, but this falls outside the scope of this preliminary presentation. In order precisely to compare experimental results with those of numerical models of nonlinear development of the turbulence, it would be useful to apply the wavelet analysis to the results of numerical simulations of several plasma instability mechanisms.

5. CONCLUSION

We have applied the wavelet analysis to turbulent electric and density waveforms that are caused by gradient-drift instability in the ionospheric plasma. This method of analysis is well adapted to the study of the small scale structures of the turbulence and in particular to the determination of its degree of inhomogeneity. Furthermore, the comparison of the wavelet transforms of the two fields belonging to the same physical phenomenon allows a determination of the relation between these fields in the time–frequency plane, and could certainly be very helpful in understanding and identifying the plasma instability mechanisms responsible for the growth of the observed electrostatic turbulence.

The method could also be applied to the analysis of two components of a vector field (electric, magnetic, velocity) and to the study of the polarization characteristics of transient signals. This will be the subject of further work.

Acknowledgements—The ARCAD-3 program, aboard the AUREOL-3 satellite, was undertaken jointly by the Centre National d'Etudes Spatiales (CNES) in France and the Space Research Institute (IKI) in Russia. We thank J. J. Berthelier and C. Béghin for providing us with electric field and electron density data, and the referee for useful comments.

REFERENCES

Basu S., Basu S., McKenzie E., Fougere P. F., Coley W. R., Maynard N. C., Winningham J. D., Sugiura M., Hanson W. B. and Hoegy W. R.	1988	*J. geophys. Res.* **93,** 115.
Béghin C., Karczewski J. F., Poirier B., Debrie R. and Massevitch N.	1982	*Ann. Geophys.* **38,** 615.
Bendat J. S. and Piersol A. G.	1971	*Random Data: Analysis and Measurement Procedures.* John Wiley, New York.
Berthelier J. J., Lefeuvre F., Mogilevsky M. M., Molchanov O. A., Galperin Y. I., Karczewski J. F., Ney R., Gogly G., Guérin C., Lévèque M., Moreau J. M. and Sené F. X.	1982	*Ann. Geophys.* **38,** 643.
Cerisier J. C., Berthelier J. J. and Béghin C.	1985	*Radio Sci.* **20,** 755.
Daubechies I.	1990	*IEEE Trans. Inform. Theory* **36,** 961.
Flandrin P.	1990a	*Proceedings of the Conference on Wavelets*, p. 68, second edition, Combes J. M., Grossmann A. and Tchamitchian P. (eds). Springer, Berlin.
Flandrin P.	1990b	*Lecture Notes in Mathematics, Les Ondelettes en 1989*, Lemarié P. G. (ed). Springer, Berlin.
Gabor D.	1946	*J. Inst. Elect. Eng.* **93,** 429.
Goupillaud P., Grossmann A. and Morlet J.	1984	*Geoexploration* **23,** 85.
Grossmann A., Holschneider M., Kronland-Martinet R. and Morlet J.	1987	*Adv. Electronics Electron Physics* **19,** 289.
Grossmann A., Kronland-Martinet R., and Morlet J.	1990	*Proceedings of the Conference on Wavelets*, p. 2, second edition, Combes, J. M., Grossmann A. and Tchamitchian P. (eds). Springer, Berlin.
Holschneider M., Kronland-Martinet R., Morlet J. and Tchamitchian P.	1989	*Proceedings of the Conference on Wavelets*, p. 286, Combes J. M. *et al.* (eds). Springer, Berlin.
Kelley M. C. and Mozer F. S.	1972	*J. geophys. Res.* **77,** 4158.
Keskinen M. J. and Ossakow S. L.	1983	*J. geophys. Res.* **88,** 474.
Kintner P. M. and Seyler C. E.	1985	*Space Sci. Rev.* **41,** 91.
Kronland-Martinet R., Morlet J. and Grossmann A.	1987	*Int. J. Pattern Recog. Artificial Intell.* **1,** 273.

MOUNIR H., CERISIER J. C., BERTHELIER A., LAGOUTTE D. and BÉGHIN C. 1991 *Ann. Geophys.* **9,** 725.
PAPOULIS A. 1977 *Signal Analysis.* McGraw-Hill, New York.
TEMERIN M. 1978 *J. geophys. Res.* **83,** 2609.
TSUNODA R. T. 1988 *Rev. Geophys.* **26,** 719.